

An embedded circumnuclear disk in Mrk 273

H.-R. Klöckner^{1,2} and W. A. Baan²

¹ Kapteyn Institute, University of Groningen, PO Box 800, 9700 AV Groningen, The Netherlands

² ASTRON, Westerbork Observatory, PO Box 2, 7990 AA Dwingeloo, The Netherlands

Received 8 January 2004 / Accepted 13 February 2004

Abstract. Radio observations using very long baseline interferometry (VLBI) and the Westerbork interferometer have been carried out to study the hydroxyl megamaser emission in Mrk 273 at different spatial resolutions. Line and continuum observations were carried out by the European VLBI network (EVN) at 1.6 GHz and display a number of distinct structural components in the central arcsec² region. The observed continuum emission shows three prominent regions with both flat and steep spectral indexes.

The hydroxyl (OH) emission detected by the EVN measurements accounts for only 12 percent of the total OH emission in Mrk 273, but it does show the same dominant 1667 MHz line emission components as the WSRT observations. The spatial distribution of the maser emission provides a high resolution view of the molecular environment in the nuclear region. The OH emission has only been detected toward a distinct radio source in the northern nucleus with a spatial extent of 108 pc. The OH emission is only partially superposed on the radio continuum and is associated with the near-infrared emission source. The low pump efficiency of the maser and the OH main-line ratio suggest that this emission originates in an optically thin and unsaturated maser environment with a complex pumping scheme that cannot be explained by radiative infrared pumping with a single dust temperature. The specific line emission pattern and the line-of-sight velocities indicate the organized structure of an edge-on disk/TORUS with a Keplerian rotation surrounding a central object with a binding mass of $1.39 \pm 0.16 \times 10^9 M_{\odot}$.

Key words. galaxies: individual: Mrk 273 – masers – galaxies: ISM – galaxies: kinematics and dynamics

1. Introduction

Extragalactic hydroxyl (OH main-lines) emission has been studied since the early eighties (Baan et al. 1982), establishing a new class of extragalactic masers with unexpected isotropic luminosities of several magnitudes higher than the most luminous galactic counterparts (e.g. W3(OH)). The OH megamaser (OH-MM) galaxies are a sub-sample of the ultra-luminous infrared galaxies (ULIRG) that are morphologically peculiar due to ongoing mergers. The nuclei exhibit phenomena related to (circum-nuclear) starburst (SBN) activity and/or the presence of an active galactic nucleus (AGN). The high molecular and dust content of the nuclear regions together with the nuclear activity render these sources ideal probes for studying the circumnuclear environment. The exceptional line width of the OH emission has been thought to exclusively trace the circum-nuclear environment close to a central power source (e.g., see Klöckner & Baan 2003). So far, only a small fraction of the prominent OH-MM galaxies has been observed by using very long baseline interferometry. These studies have shown a rather complex picture of continuum and the maser emission inside the nuclear region (for a detailed list see Klöckner & Baan 2002).

The galaxy Mrk 273 (UGC 08696, IRAS 13428+5608) has been classified as a ULIRG with an infrared luminosity of $L_{\text{FIR}} = 1.208 \times 10^{12} L_{\odot}$. Its warm infrared color (ratio of the 60 μm to 100 μm IRAS flux of 1.02) suggests that the bulk of the infrared excess is associated with dust heated by nuclear star formation rather than by a dominant contribution of an accretion disk (Sanders & Mirabel 1996, and references therein). In the optical Mrk 273 displays a morphologically disturbed structure with a thin tidal tail extending towards the south by 50 arcsec (1.3 arcsec \sim 1 kpc)¹ and a fan-like plume. The infrared excess, the distinct morphology and the observed soft X-ray halo of $\sim 50'' \times 30''$ indicate a merger event within the last 10^8 yrs (Knapen et al. 1997). The fan-like plume itself is 15'' in size and has a rather complex structure consistent with the inner interaction region in a galactic merger. The central region of Mrk 273 harbors prominent dust lanes, ionized gas, and several sources visible at different emission bands, which complicates the diagnosis of the nuclear energetics. Strong optical emission lines from two distinct regions indicate the presence of a low-luminosity LINER nucleus in the north with a size of around 1 arcsec and a Seyfert 2 nucleus located 4 arcsec towards the southwest (Colina et al. 1999).

¹ The optical redshift of $z = 0.03778$, $q_0 = 0.5 \text{ km s}^{-1}$ and $H_0 = 75 \text{ km s}^{-1} \text{ Mpc}^{-1}$ are used for all further estimates in this paper; therefore 1 mas corresponds to 0.7389 pc.

Send offprint requests to: H.-R. Klöckner,
e-mail: hrkloeck@astro.rug.nl

The LINER source in the north reveals both diffuse and compact radio emission components, which support the notion of enhanced star formation as well as the optical classification (Carilli & Taylor 2000). On the other hand, hard X-ray emission has only been detected towards this source, which indicates either a heavily obscured high-luminosity AGN or a less obscured low-luminosity AGN as a nuclear power plant (Xia et al. 2002). The kinematical structure of this northern source has been well studied at various resolutions using [O III], HI, CO, and OH line emission. These observations give evidence of a disk-like structure of less than 800 mas in size (Colina et al. 1999; Schmelz et al. 1987, 1988; Downes & Solomon 1998).

The southern Seyfert 2 source shows enhanced emission in the near-infrared (NIR), only soft X-ray emission, and almost no emission in the radio, which indicates either another dust enshrouded AGN or the possible interaction region of an ionization cone of the northern nucleus (Knapen et al. 1997; Xia et al. 2002). Radio observations of the central part of Mrk 273 reveal one additional object to the south-east of the northern nucleus, which has no NIR counterpart and no hard X-ray emission. However, this source does show a distinct jet-like morphology in the radio and displays faint HI absorption and CO emission indicating a possibly outflow from one additional nucleus into the surrounding ISM (Knapen et al. 1997; Downes & Solomon 1998; Carilli & Taylor 2000).

New WSRT and EVN observations of the OH line and the continuum emission in the Megamaser galaxy Mrk 273 are presented in this paper. The OH emission structure at the northern nucleus and the continuum structure are used to understand the kinematics and the physical properties of the environment in the nuclear region.

2. Observations and data reduction

The hydroxyl line- and continuum emission in Mrk 273 was observed with the Westerbork Synthesis Radio Telescope (WSRT) and the European VLBI Network (EVN). The observations reveal structures spanning scale sizes of about three orders of magnitude ranging from galactic to nuclear scales.

The WSRT observations were made on 7 February 2002 with two hours of on-source observations and respectively 3 and 4 min on the calibrator 3C 286 at the beginning and the end of the on-source observation. The dual polarization line observations had a bandwidth of 20 MHz using a rest frequency between the two hydroxyl main lines (1666 MHz) and a heliocentric velocity of 11 326 km s⁻¹. The set-up with 256 channels gave a velocity coverage of about 3734 km s⁻¹ and a velocity resolution of about 14.6 km s⁻¹ per channel. At the source distance, the OH emission lines are red-shifted out of the protected band and into the band where the GLONASS global positioning satellite system operates. As a result considerable radio frequency interference (RFI) was encountered in the measurements. The cross correlation products produced by the WSRT interferometer were used to eliminate the influence of RFI on the data. The amplitude and gain calibrations were performed after applying the Tsys measurements to the data. The RFI-affected data set of the calibrator source was excised iteratively with an automated calibration and flagging

procedure based on individual tasks from the Astronomical Imaging Processing System (AIPS). After final editing of the calibrator, the phases and the band-pass corrections (frequency dependent gains) were used to calibrate the dataset of the target source. Final RFI excising of the data of the target source was performed using the same automatic excising method (for a detailed description see Klöckner 2004). Observations of a few hours with the east-west WSRT array result in a relatively poor UV-coverage and detailed imaging was not carried out using this dataset. After applying all corrections to the data set of the program source, a Total-Power emission spectrum was produced from the data in the UV plane (see Fig. 3).

The EVN observations of Mrk 273 were made on 10 February 2000 using seven antennae Effelsberg, Onsala (85 ft), Jodrell Bank (Lovell), Medicina, Noto, Torun and the phased WSRT array. Due to weather and technical problems only half of the scheduled 12 h observation have been used. The data were processed with the correlator at the Joint Institute for VLBI in Europe (JIVE) in Dwingeloo. To observe both OH main-line emissions (1667 and 1665 MHz), the band pass was centred at a mid frequency of 1666.38 MHz and assuming a optical heliocentric velocity of 11 350 km s⁻¹. The observations used a total bandwidth of 8 MHz covering a velocity range of 1494 km s⁻¹ in two polarizations, 256 channels and 2 bit correlation, which leads to a velocity resolution of 5.8 km s⁻¹ per channel in the source rest frame. The observation was performed in phase referencing mode, using a 13 min (10 + 3 min) cycle to cover the target source Mrk 273 and the phase-calibrator source J 1337+5501. The projected telescope spacings lead to a synthesized beam width of minimal 30 mas. Data reduction and analysis was performed using AIPS in combination with routines from the Groningen Image Processing System (GIPSY). Before standard calibration of the UV-dataset were performed, new accurate positions were applied for those telescopes that are not part of the geodetic network (Charlot et al. 2002). The observational data was a-priori gain calibrated by using the system temperatures measured at each individual telescope. The phases were then calibrated by initial fringe finding followed by a full self-calibration procedure on the phase calibrator. The bandpass of the system was calibrated by using the phase-calibrator source, because no simultaneous measurement at all telescopes of the scheduled band pass calibrator (3C 286) had been recorded. Further improvement of the calibration could be achieved by performing an additional self-calibration procedure on the channel with the highest line flux and applying these phase corrections to the other channels. Imaging of the line and continuum emission was produced after applying the final calibration to all channels in the UV-dataset.

3. Results

3.1. Radio continuum

The low-resolution (14'') continuum flux density at 1660 MHz was obtained from the off-line emission in the WSRT spectrum to be 102 mJy. This value is 13 to 22 percent lower than the catalogued estimates of the NVSS and the FIRST databases at

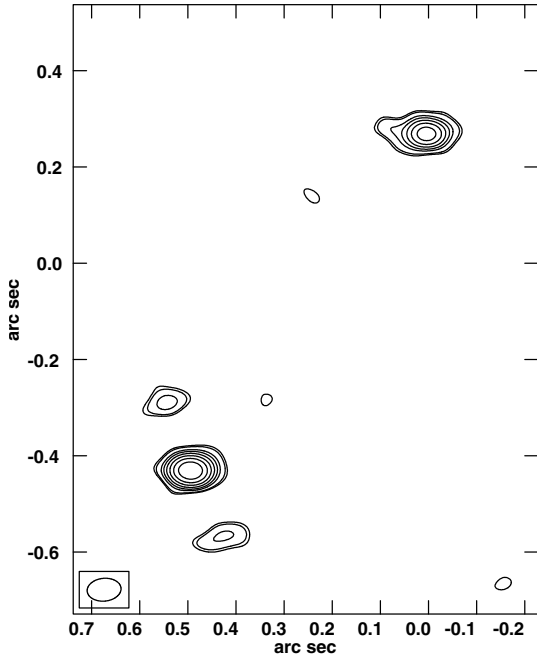


Fig. 1. Continuum emission structure of Mrk 273 at 1.6 GHz observed on 10 February 2000 using the EVN network including the telescopes Effelsberg, Onsala (85), Jodrell Bank (Lovell), Medicina, Noto, Torun and the phased WSRT array. The measurements were mapped by averaging the offline spectral channels, applying natural weighting, and tapering, that leads to a spatial resolution of 71×47 mas oriented at 68.7° . The highest peak flux of 3.392 mJy per beam corresponds to the southeast source. The contour levels are in a geometric progression of $\sqrt{2}$; hence every two contours imply a factor of two in surface brightness. The first contour is 0.15 mJy beam $^{-1}$ corresponding to a 3.9σ level.

1.4 GHz. Although the catalogue images display unresolved point sources, they also show differences in continuum flux densities on scale sizes between their spatial resolution of $5.4''$ and $45''$. This could indicate the presence of a low brightness temperature continuum structure on a scale size between these spatial resolutions. The flux discrepancy with the WSRT observations could indicate a steep spectral index of Mrk 273 or it is caused by the influence of RFI, which would lead to an increase of the system temperature and a reduction of the continuum level. The low resolution NVSS radio data was compared with the catalogued infrared emission. The resulting q -value defined as $\log(L_{\text{FIR}}/L_{\text{radio}})$ of 2.28 is slightly lower than the values typically seen in star-forming galaxies, which indicates that any radio core and radio jet or lobe component only make a minor contribution to the total radio emission of Mrk 273 (Yun et al. 2001).

The complex continuum structure in the central region of 1 square degree of Mrk 273 has been studied in previous observations. The continuum structure presented in Fig. 1 displays multiple sources matching the known northern and south-eastern structures in the nuclear region (natural weighted data set of 71×47 mas resolution). The south-eastern component splits into a marginally resolved triple source at position angle $\text{PA} \sim 25^\circ$. In the uniform weighted map at a slightly higher resolution of 41×34 mas, the southern source of this triple

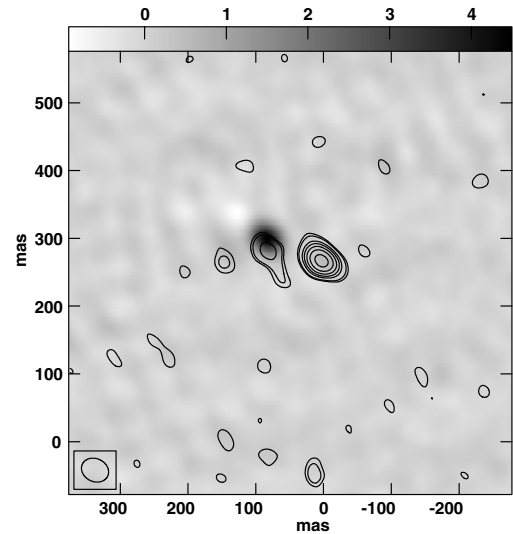


Fig. 2. Continuum emission superposed on the integrated OH line emission observed in Mrk 273 by the EVN. A close-up of the northern nucleus shows the continuum emission in contours superposed on the integrated line emission in grey-scale color-coding. The dataset was uniformly weighted, which results in a 41×34 mas resolution oriented at 64.3° . The contour levels are a geometric progression in the square root of 2 starting at 0.15 mJy beam $^{-1}$. Note that the line- and continuum emission displayed here may not fully justify the scenario of the classical OH Megamaser model, where the line emission would be located in front of the continuum emission (Baan 1989).

structure reveals two emission components, whereas the northern source remains unresolved. The observed emission structures are consistent with existing VLBA observations of the south-eastern region (1.3 GHz) at somewhat lower resolution of 50 mas (Carilli & Taylor 2000). Therefore, the EVN data partially trace the organized structure of the southeast source comprising an amorphous double jet of 370 mas in extent. The central source has a brightness temperature on the order of 10^5 K, and is characterized by a relatively flat spectral index (α , $F \sim \nu^\alpha$) between 1.6 and 5 GHz of 0.26 ± 0.05 (5 GHz data taken from Knapen et al. 1997). Similar values have been found in a sample of ULIRGs, which suggests that synchrotron emission could be the dominant emission process in such sources (Crawford et al. 1996).

The continuum emission in the northern source of the nuclear region in Mrk 273 shows an east-west elongated structure of 213 mas in size (Fig. 1). At the resolution of 41×31 mas, the northern radio emission (Fig. 2) splits into two components spatially separated by 77 mas in east-west direction. Each component shows a brightness temperature on the order of 10^5 K. The western component is somewhat brighter and slightly extended towards $\text{PA} = -33^\circ$, whereas the emission at the eastern component fades towards the south. Similar characteristics for both continuum components have been found with the VLBA + VLA at 1.3 GHz, which have a slightly higher brightness temperature (Carilli & Taylor 2000). Observations at 5 GHz with the MERLIN array, with a resolution that is almost comparable to that of the present EVN data, show enhanced continuum emission at the eastern source as compared with the western source, which trend is also seen in the NIR emission

(Carilli & Taylor 2000; Knäpen et al. 1997). The spectral index of both continuum sources is rather different between 1.6 and 5 GHz with values of $\alpha_{\text{east}} = 1.5 \pm 0.4$ and $\alpha_{\text{west}} = 0.01 \pm 0.12$, respectively. The flat spectrum suggests purely thermal emission possibly caused by photo-ionization of the ISM by star formation. While a steep spectrum at the eastern source would indicate free-free absorption of the thermal emission or the synchrotron emission, the radio continuum at these frequencies does not provide clear clues of the nature of the nuclear engine (Condon 1992). Comparing the structures observed with the EVN with images obtained by the VLBA + VLA array at 1.3 GHz shows that these EVN observations, even with very poor UV-coverage at short baselines, trace the inner part of the structures in the northern nucleus of Mrk 273 (see Fig. 2 in Carilli & Taylor 2000). The VLBA+VLA datashow both sources to be embedded in a diffuse emission structure extending over 500×300 mas.

3.2. The line emission

It has become known that for extragalactic OH maser sources only a small fraction of the total OH emission can be detected by observations at parsec resolution. The high resolution EVN measurements for Mrk 273 reveal only 12 percent of the hydroxyl emission at low resolution obtained using the WSRT (Figs. 3 and 4). A detailed comparison of the individual line emission component presented in Fig. 7 shows that the central 1667 MHz line may account for some 85% of the EVN data, whereas the broader emission features could not be recovered at all. The properties of the individual line emission components have been listed in Table 1.

Extragalactic hydroxyl masers generally show dominant 1667 MHz emission and are accompanied by weak (or sometimes non-existent) 1665 MHz line emission. At low resolution the OH spectrum shows three features covering a total velocity range of 1257 km s^{-1} . Such exceptional velocity ranges have also been seen in other Megamaser galaxies that are characterized by a violent circum-nuclear environment such as Arp 220, IRAS 14070+0525, and III Zw 35 (Baan et al. 1989, 1992; Pihlström et al. 2001). The large velocity range of the observed hydroxyl emission at WSRT scales complicates the identification of individual line features with one of the hydroxyl transitions. The theoretical velocity offset of both maser lines is 365.6 km s^{-1} at the assumed redshift of Mrk 273 of 0.03778 and in the reference frame of the 1667 MHz line. Therefore, line features up to about 11400 km s^{-1} will certainly be 1667 MHz features, whereas the line features around 11600 km s^{-1} could be associated with the 1665 MHz OH main line. The WSRT spectrum indicates a 1667/1665 MHz main-line ratio of about 1.7, which is close to the 1.8 local-thermodynamic-equilibrium (LTE) value.

The line emission feature at the lowest velocity has been seen in the early observation but has not been identified as such in the literature² (first detected by Staveley-Smith et al. 1992).

² Not taking this particular line emission feature into account in the observational set-up will cause systematic errors for the kinematics and the OH content of low resolution investigations of the hydroxyl emission in Mrk 273.

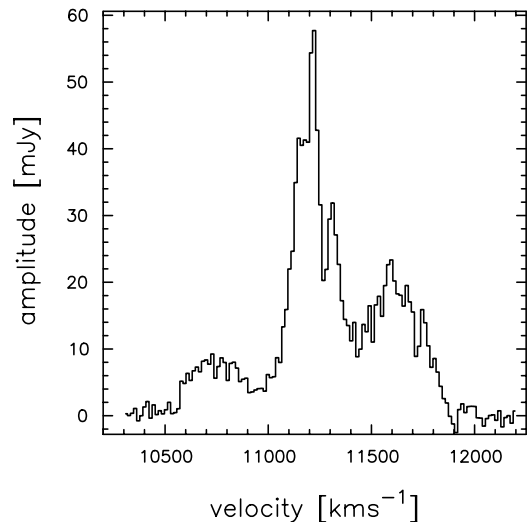


Fig. 3. Integrated line emission spectrum of Mrk 273 observed with the WSRT. The spectrum has a velocity scale corresponding to a heliocentric velocity of the 1667 MHz line and a spectral resolution of 14.6 km s^{-1} . In order to compare this 20 MHz bandwidth observation with the high resolution EVN spectrum of Fig. 4, the velocity range has been cut off at 12250 km s^{-1} . A continuum flux density of 102.6 mJy has been subtracted from the emission line spectrum. The enhanced line feature at a central velocity of about 11326 km s^{-1} corresponds to the 1667 MHz main-line emission, whereas predominately the emission at $+365.6 \text{ km s}^{-1}$ velocity offset is related to the 1665 MHz main-line emission (see Figs. 4 and 7).

This component centred at 10773 km s^{-1} and with a width of about 380 km s^{-1} complicates the interpretation of the maser emission as it highlights gas at a non-systemic velocity. The sub-structure of the main emission line at a velocity of around 11200 km s^{-1} shows three distinct components. The broad features at 11600 km s^{-1} has a line width of 334 km s^{-1} (*FWHM*), which is incidentally of the same order of magnitude as that of the broad line at 10773 km s^{-1} .

The EVN measurements in Fig. 4 show a less complicated emission spectrum because some of the broad emission has disappeared and the emission features can be easily associated with the two hydroxyl transitions. The velocity range of the emission at this resolution is 484 km s^{-1} , which is one third of the observed velocity range at WSRT resolution. The spectrum displays strong emission features at 11200 km s^{-1} associated with the 1667 MHz line and a weak emission line at 11600 km s^{-1} . The clear triple structure of the strong 1667 MHz emission changes dramatically as the fluxes of the f2 and f4 features are reduced at higher resolution (Table 1). The weak emission feature (f5) at 11600 km s^{-1} can be identified as 1665 MHz emission using the velocity offset of 369.9 km s^{-1} relative to the strongest 1667 MHz line feature f3.

At a spatial resolution of a few milli-arcsec of the EVN data, the OH emission has been found exclusively toward the northern source of the nuclear region in Mrk 273 (see Fig. 2).

The OH emission structure has an extent of 146 mas and partially covers the eastern continuum component. A marginal (3.5σ) line emission component at 11326 km s^{-1} and a line

Table 1. Properties of the individual emission line features obtained by the WSRT and the EVN interferometers. The emission line features are sorted by increasing centre velocity, corresponding to the heliocentric velocity of the 1667 MHz emission line. The velocity estimates have systematic errors of 14.6 and 5.8 km s⁻¹ respectively, that are related to the different spectral resolutions of the measurements. A reduced chi-square fit has been used to estimate the individual properties of the Gaussian shaped line profiles. The theoretical velocity difference of the two OH main lines in the reference frame of the 1667 MHz line is 365.6 km s⁻¹ at the redshift of Mrk 273. The estimated velocity difference of the line features f3 and f5 match the theoretical offset within a systematic error of one channel, indicating that they are a pair of hydroxyl main-lines.

	WSRT	EVN
– f1 component –		
center velocity _{f1} [km s ⁻¹]	10773.3	...
peak flux _{f1} [mJy]	7.84 ± 0.57	...
<i>FWHM</i> _{f1} [km s ⁻¹]	378.84 ± 36.05	...
<i>L</i> _{f1} [<i>L</i> _⊙]	106.99 ± 12.78	...
– f2 component –		
center velocity _{f2} [km s ⁻¹]	11 161.8	11 168.0
peak flux _{f2} [mJy]	39.34 ± 1.00	11.63 ± 0.43
<i>FWHM</i> _{f2} [km s ⁻¹]	128.64 ± 4.44	51.79 ± 2.75
<i>L</i> _{f2} [<i>L</i> _⊙]	195.41 ± 8.38	23.28 ± 1.51
– f3 component –		
center velocity _{f3} [km s ⁻¹]	11 223.3	11 224.4
peak flux _{f3} [mJy]	33.74 ± 1.74	33.93 ± 0.67
<i>FWHM</i> _{f3} [km s ⁻¹]	44.4 ± 2.70	29.9 ± 0.77
<i>L</i> _{f3} [<i>L</i> _⊙]	58.47 ± 4.66	39.60 ± 1.23
– f4 component –		
center velocity _{f4} [km s ⁻¹]	11 314.2	11 299.8
peak flux _{f4} [mJy]	25.80 ± 1.16	5.24 ± 0.28
<i>FWHM</i> _{f4} [km s ⁻¹]	90.97 ± 5.57	114.86 ± 11.23
<i>L</i> _{f4} [<i>L</i> _⊙]	93.05 ± 7.07	0.92 ± 0.27
– f5 component –		
center velocity _{f5} [km s ⁻¹]	11 594.6	11 594.3
peak flux _{f5} [mJy]	19.76 ± 0.60	2.71 ± 0.51
<i>FWHM</i> _{f5} [km s ⁻¹]	334.56 ± 14.16	30.88 ± 6.75
<i>L</i> _{f5} [<i>L</i> _⊙]	274.87 ± 14.32	3.48 ± 1.00

width of 54 km s⁻¹ (*FWHM*) has been detected toward the western continuum component. The centroid of the line emission at the eastern source is displaced about 23.2 mas towards the north relative to the continuum emission (Fig. 5). There is an asymmetry in the intensity of the line features f2 and f4 that is most likely caused by the association of feature f2 with the northern part of the continuum emission serving as a background for maser amplification. A comparison of the properties of the individual OH line components in Table 1 shows that the EVN data accurately traces the most compact and dominant OH emission seen towards Mrk 273.

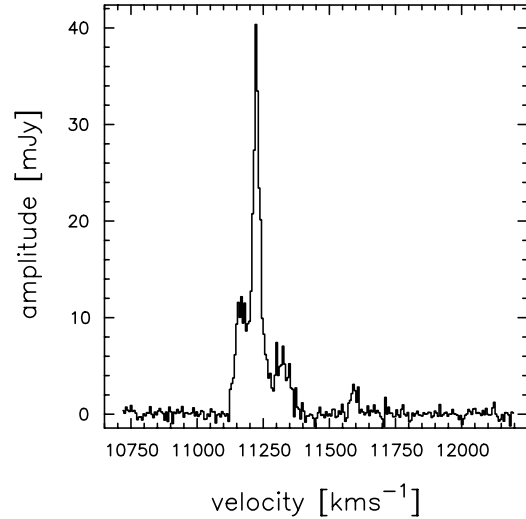


Fig. 4. Integrated line emission spectrum of Mrk 273 observed with the EVN. The spectrum has a velocity scale corresponding to a heliocentric velocity of the 1667 MHz line and a spectral resolution of 5.6 km s⁻¹. Note that the velocity cutoff at higher velocities corresponds to the cutoff in Fig. 3. The strong line features displayed here correspond to the 1667 MHz main-line emission and the weak emission line is related to the 1665 MHz main line. The expected velocity difference between the OH main-line transitions in the velocity frame of the 1667 MHz line is +365.6 km s⁻¹ at the redshift of Mrk 273.

4. Discussion

4.1. Understanding the hydroxyl emission

The hydroxyl emission in Mrk 273 displays characteristics that are typical of extragalactic OH Megamaser sources, where at high spatial resolution only a small fraction of the low resolution hydroxyl emission is detected (Lonsdale et al. 1998; Diamond et al. 1999; Klöckner et al. 2003). The excitation mechanism of the OH molecules in Mrk 273 is most likely a radiative pump provided by the infrared radiation field similar to the conclusions for other OH-MM (Baan 1989; Henkel & Wilson 1990; Skinner et al. 1997).

Mrk 273 exhibits two distinct near-infrared emission regions at arcsec-scales (south-west and north) with slightly stronger emission towards the northern nuclear source where also the OH emission has been detected (Knapen et al. 1997). By using the ratios of the individual near-infrared measurements of the two sources in Mrk 273, the infrared excess seen towards the northern source is estimated to be $5.96 \times 10^{11} L_{\odot}$. Considering the spectral width of the OH emission (e.g. $r_{\text{OH}} = 6.73$ MHz) and the applying this to the infrared emission (r_{FIR}), a lower limit of the OH pumping efficiency can be estimated using the following ratio:

$$P_{\text{OH}} = \frac{L_{\text{OH}} \times r_{\text{FIR}}}{L_{\text{FIR}} \times r_{\text{OH}}}, \quad (1)$$

where L_{OH} and L_{FIR} are the luminosities. The large scale OH emission in Mrk 273 shows a pump efficiency of the order of 0.29 percent. An upper limit for the efficiency of 0.40% can be found by using the maximum infrared flux of the pump transition being closest to the black body peak and the maximum

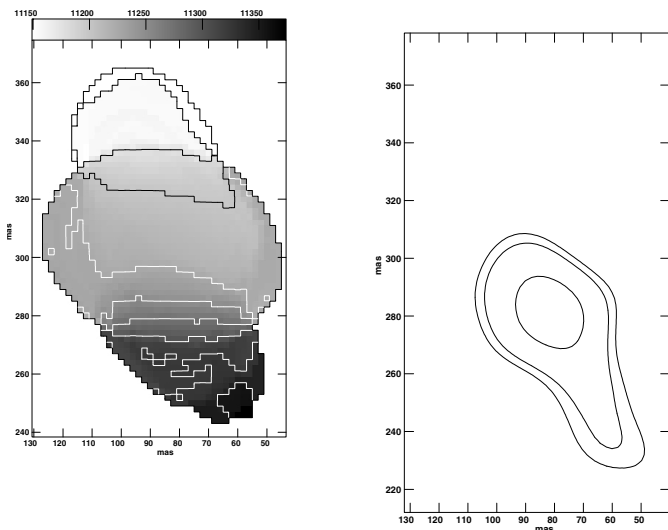


Fig. 5. The velocity field and the structure of the 1667 MHz OH emission and the structure of continuum emission seen in a close-up of the northern nucleus in Mrk 273. The spatial resolution is identical to Fig. 2 and the velocity scale is the same as in Fig. 4. The velocity field of the OH 1667 MHz emission is shown in grey scale covering a velocity range between 11 150 and 11 350 km s⁻¹ and contours are separated by 25 km s⁻¹. A north-south velocity gradient of 1.62 km s⁻¹ per mas is observed (2.19 km s⁻¹ pc⁻¹), where the northern side moves towards the observer. Only the OH lines located in the centre and the southern edge of the disk are superposed on the observed continuum emission.

peak flux of the observed OH line emission (for the OH transitions see: Destombes et al. 1977). Nevertheless, in both cases the low pump efficiency indicates an unsaturated maser process. Because the maser emission would be saturated if every available pumping event (in this case a infrared photon) produces a maser photon with an efficiency that depends only on the details of the pumping scheme (see p. 81: Elitzur 1992). Saturation would occur when the measure of amplification by the maser process directly affects the pumping efficiency. The ratio γ of the maser intensity at with saturation takes place in the 1667 MHz hydroxyl line is about unity:

$$\gamma = \frac{I_{\text{sat}}}{I_{\text{unsat}}} \sim \frac{P_{\text{OH}}\Gamma}{A_{2-2^+}}, \quad (2)$$

where I_{sat} is the intensity at saturation of the maser, I_{unsat} is the unsaturated maser intensity, A_{2-2^+} the Einstein coefficient of the 1667 MHz transition, P_{OH} is the efficiency as defined above, and Γ is the loss rate. The loss rate Γ is generally of the same order as the collision rate. For OH in HI regions, it has been shown that the OH-ion interaction is the most important collision process, which leads to a collision rate of $37 \times 10^{-9} N_{\text{HI}}$, where N_{HI} is the hydrogen density (Rogers & Barrett 1968). The hydrogen density is not generally known but it can be estimated using the molecular hydrogen abundance. The abundance of the molecular hydrogen has been dynamically modeled for Mrk 273 to be 1860 H₂ molecules per cm⁻³ in the northern nucleus (Downes & Solomon 1998). The relative abundance of HI to molecular hydrogen is assumed to be similar to the galactic value of 20 (valid for the inner 300 pc in

the Milky Way; Güsten 1989). For a saturation ratio $\gamma = 1$, the natural logarithm of the gain threshold for maser amplification in Mrk 273 as expressed in Eq. (2) is 10.8; above this value saturated maser emission is expected. The saturation parameter can be estimated observationally by determining the optical depth from either the maser main-lines or one maser line in combination with the continuum emission (for an explanation see Henkel & Wilson 1990; Goss 1968). Since a clear separation of the two OH main lines is not possible for the WSRT observation, an upper limit on the gain of -0.43 can be estimated using the continuum and the peak flux of -0.43 of the 1667 MHz line emission. An additional constraint on the amplification process can be made using the low resolution WSRT OH data and assuming that the radio continuum observed in the northern source serves as a background for the more diffuse OH emission, which is missed at the resolution of the EVN. The continuum emission in the northern source in Mrk 273 has been imaged in detail with the VLBA, showing a diffuse continuum structure being punctuated by a number of compact sources (SNRs) with brightness temperatures larger than 3×10^6 K (Carilli & Taylor 2000). The maximal brightness temperature of the diffuse maser emission can be estimated from the missing line emission features in the EVN data and the corresponding features in the MERLIN observation (Yates et al. 2000). The diffuse maser emission that is not seen by the EVN observations accounts for brightness temperatures of the order of 4×10^5 K. Within the classical OH maser amplification model, these assumptions suggest a maximal gain of about 2.01, which is significantly lower than the estimated saturation threshold (Baan 1989, 1985; Baan et al. 1982).

A further constraint on the nature of the maser emission follows from evaluating the level populations to estimate the main-line ratios. Since the excitation mechanism of the OH molecules is most likely radiative pumping, the integrated infrared emission field determines the OH main-line ratio. Assuming a spectral-temperature of a single black-body or a single grey-body, the population in the OH ground level ($^2\Pi_{3/2}$) follows from the population cascade of the rotational and vibrational levels (Destombes et al. 1977). By solving the rate equations for the individual levels up to $J = 9/2$, a gray-body temperature of 63 K and a black-body temperature of 68 K suggest a main-line ratio ranging from 1.98 or 3.00, respectively (note that for the gray body estimate additional infrared data has been used from Klaas et al. 2001). It has been mentioned that the extreme kinematics in Mrk 273 will affect the diffuse OH main-line emission and the main-line ratio, which may lead to systematic errors. Nevertheless, the velocity difference of the individual f3 and f5 features suggests that these are a line pair. At low resolution their line ratio is 1.71 (see Table 1), which is close to the LTE value of 1.8 and can not be explained by an infrared pumping scheme. At high resolution in the EVN data, the main line ratio is 12.5 based on a clear identification of both OH lines, which is a value that cannot be produced by the infrared radiation field with a single spectral temperature. Therefore, in order to obtain a detailed model of the observed line ratios, detailed modelling of the radiation field and of the level populations needs to be employed, which will be done elsewhere. The overall maser emission process

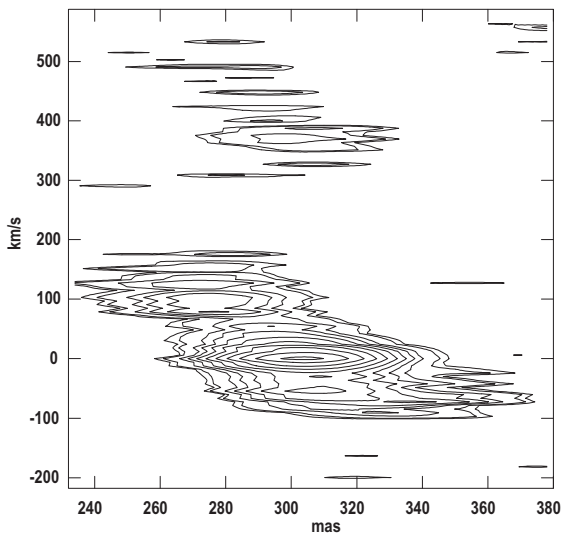


Fig. 6. The position-velocity structure of the hydroxyl emission in the northern part of Mrk 273 observed with the EVN. The main-line hydroxyl emission is displayed across the major axis of the eastern sources at spatial resolution of 41×34 mas (see Fig. 2). The dominant emission structure in the bottom part of the frame corresponds to the 1667 MHz line features. The weaker emission in the upper part of the frame displays the kinematics traced by the 1665 MHz emission. The velocity on the vertical axis corresponds to the heliocentric velocity of the 1667 MHz line emission. The declination refers to the central position, which is consistent with all figures presented here. The centre velocity is $11\,222.3$ km s $^{-1}$ and the contours are in steps of 3 starting at 0.75 mJy beam $^{-1}$.

can thus be further constrained to be an unsaturated maser, because for a saturated maser the process would only depend on the details of the infrared pumping scheme.

The OH emission at EVN resolution as shown in Fig. 2 only shows enhanced maser emission at the eastern source, where the NIR emission is a factor 2 stronger relative to the western source (Knapen et al. 1997). Since the dominant pumping lines of the OH molecule fall in the NIR, a strong OH maser versus FIR dependence could be expected. A similar connection has been found for Arp 220, where a diffuse emission structure follows the NIR intensity contours (Baan & Haschick 1984). The spatial distribution of the continuum emission and of the OH emission suggests that the diffuse continuum emission serves as a background for the amplification. The difference in intensity of the f3 and f4 1667 MHz line features is possibly caused by the difference in background continuum at these locations. The location of the individual line features with respect to this continuum emission follows from the velocity field shown in Fig. 5.

A clear discrimination of the OH main-lines and still small systematic errors in determining the line ratios may lead to an accurate estimate of the OH column density. Assuming that both main-line components f3 and f5 and the continuum originate along the same line of sight, the optical depth of the OH can be estimated to be $\tau_{\text{unsaturated}} = -3.20$, which corresponds to a column density of $N_{\text{OH}} = 4.58 \times 10^{14} T_{\text{ex}} \text{ cm}^{-2}$ (for explanation see Goss 1968). An estimate of the optical depth also follows from a comparison of the continuum emission

and the properties of f3 leading to the apparent optical depth of -4.30 (the different ways of estimating the optical depth are described in Henkel & Wilson 1990). Combining these estimates for the optical depth suggests a covering factor of 0.32, that accounts for how much the OH emission clouds cover the underlying continuum emission. Altogether, the pumping efficiency, the infrared emission, the optical depth, and the estimate of the saturation threshold indicate that the hydroxyl emission in Mrk 273 is spatially extended between a thousand and a few tens of parsecs and is explained by an unsaturated maser emission process.

4.2. The nuclear kinematics

The combination of OH data from the EVN and the WSRT traces the hierarchical structure of the circum-nuclear environment from a few tens of parsec up to kilo parsec scales in the northern nucleus of Mrk 273. The kinematical pattern has been imaged using several molecular tracers leading to a gas disk hypothesis for the northern nucleus (Cole et al. 1999; Downes & Solomon 1998). In particular, MERLIN imaging of the neutral hydrogen absorption at spatial resolution of 200 mas shows a nuclear disk of about 800 mas in extent. The kinematics of this disk is explained by solid-body rotation with an velocity gradient of about 1.39 ± 0.003 km s $^{-1}$ per mas (1.88 km s $^{-1}$ pc $^{-1}$) in east-west direction (Cole et al. 1999). On the other hand, MERLIN data of the OH emission at a similar resolution displays a rather complicated picture in which individual maser clumps do not provide any clear indication of a disk structure at similar scale sizes (Yates et al. 2000). At a resolution comparable to that of the EVN observations (see Fig. 5), the VLBA HI data show that the northern nucleus is spatially resolved showing a 500×300 mas extended disk traced by HI in absorption with a slightly lower velocity gradient of 1.5 km s $^{-1}$ per mas (2.0 km s $^{-1}$ pc $^{-1}$) east-west direction than the OH and with an apparent flattening of the velocity at larger radii (Carilli & Taylor 2000). The OH emission in the current EVN data is unexpectedly different from the earlier data in that the velocity gradient is north-south along the major axis of the emission (Fig. 2). Apparently the OH traces a sub-structure in the nuclear region that has emission velocities similar to those of the HI at lower resolution. At the location where the OH emission indicates a clear north-south gradient (see Fig. 5), the HI absorption shows a flaring velocity field associated with distinctly different kinematics.

The kinematical pattern of the OH line emission is shown in the position-velocity (PV) diagram in Fig. 6 and displays two almost similar velocity patterns for each of the OH main-lines transitions. The features at the bottom of the PV-diagram represent the three major components of the 1667 MHz line as seen in Fig. 4. The velocity structure shows an organized velocity field of Keplerian rotation around a central object with no evidence of flattening at larger distances. The spatial extent and the overall north-south velocity leads to a gradient of 1.62 ± 0.37 km s $^{-1}$ per mas (2.19 km s $^{-1}$ pc $^{-1}$), which is of the same order of magnitude as the MERLIN and VLBA estimates for the east-west gradient in HI. The same velocity pattern

repeats with significantly lower intensity in the upper part of the PV-diagram, where the 1665 MHz line is found.

The specific emission pattern of the OH emission (in particular of the 1667 MHz line) with a bright centre feature and two weaker components at the edges is related to the maser amplification itself. We note that the relative amplification of the maser emission is proportional to the ratio of the OH column density over the OH velocity dispersion (e.g., see: Greenhill et al. 1995). In order to simulate the representative emission pattern seen in the EVN spectrum in Fig. 4, a 3-dimensional disk and torus geometrical structure has been modelled in order to solve for the line-of-sight maser amplification. In these geometries the amplification is calculated on the basis of randomly distributed maser clouds within the disk. To produce the smooth emission line spectrum that is common for all OH Megamaser galaxies, each individual OH cloud needs to be extended and exhibit internal velocity dispersion or turbulence. For a 107.9 pc (146 mas) extended structure and an enclosed mass on the order of $1.39 \pm 0.16 \times 10^9 M_{\odot}$, the kinematics of a solid body rotation, suggested by the HI absorption measurements (Cole et al. 1999), does not account for the spectral signature and the velocity range traced by the observed line features f2, f3, and f4. The specific triple structure of the OH 1667 MHz line emission can only be reproduced by either a disk or a torus structure with Keplerian kinematics and seen almost edge-on with deviations in the inclination of less than 10° (for the dependence of the spectral signature of maser emission on geometry and the line-of-sight, see Klöckner 2004).

Therefore, the OH emission line traced by the EVN observations is explained by an almost edge-on disk or torus with Keplerian kinematics placed at PA = -15° of the eastern source in the northern nucleus of Mrk 273.

At larger scale sizes the MERLIN data of the OH emission show no clear kinematical pattern. On the other hand, the WSRT spectrum (Fig. 3) shows an emission feature (f1) blue-shifted by about 450 km s^{-1} . The presence of this feature could indicate a more disturbed environment and may explain the complicated emission pattern in the MERLIN data. Because of the large velocity range of the OH emission this feature did not get recognized in earlier observations. Since no imaging data of this OH feature is available, only an indirect comparison with optical spectroscopy could be made. The OIII line emission shows two distinct lines with different energetics at the northern nucleus (note that the spatial resolution of the reported observations is about $0.9''$, Colina et al. 1999). One OIII component indicates a highly ionized gas phase with a rather disturbed velocity field and velocity components predominantly 600 km s^{-1} blue-shifted. This velocity shift is almost in agreement with the velocity difference seen for the OH feature f1 traced by the OH emission. The other OIII line component indicates low-excitation gas that traces a rather organized velocity field oriented in east-west direction. The orientation and the velocity range of about 2400 km s^{-1} indicate that this line traces nuclear kinematics similar to those derived by radio observations at comparable resolution (Colina et al. 1999; Cole et al. 1999).

The OH emission seen in Mrk 273 is possibly associated with both the high and the low energy gas phase in the

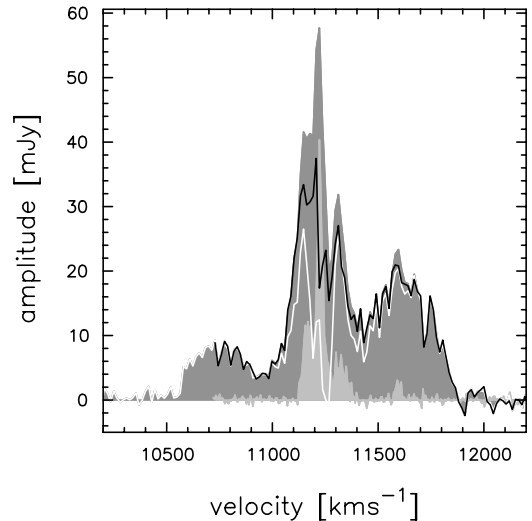


Fig. 7. A comparison of the integrated line emission spectra of the hydroxyl emission observed in Mrk 273. The dark gray shaded region displays the WSRT spectrum and the light gray shaded region the EVN spectrum. The solid black line displays the difference between the WSRT and the EVN measurements, while neglecting the different spectral resolution of these observations. The solid white line represents the difference of both observations, where the EVN spectrum, with a spectral resolution of 5.6 km s^{-1} , is smoothed to the WSRT resolution of 14.6 km s^{-1} .

northern nucleus. The broad blue-shifted OH and optical emission lines are most likely associated with a starburst driven molecular outflow. Such a scenario has been proposed and observed in other OH Megamaser sources such as Arp 220 or III Zw 35 (Baan et al. 1989). If a molecular outflow takes place, the OH molecules must be contained in some dusty layer expanding from the nuclear starburst traced in the radio continuum (Carilli & Taylor 2000). The symmetry of the residual spectrum seen in Fig. 7, where the EVN emission is subtracted from the WSRT emission spectrum would then account for the diffuse OH component on scale sizes of a few hundreds of parsec. The kinematics, the source extent, and the enclosed mass estimates of the HI absorption lines can be used to model the line-of-sight amplification of the maser clouds embedded in a circular layer and their spectral signature. Such a setup results into two distinct spectral line features at both edges of the spectrum, each having a velocity dispersion of a few hundreds km s^{-1} and covering a similar velocity range as the residual OH emission (Fig. 7). Therefore, the OH spectrum at velocities higher than systemic would show a superposition of both OH main-lines (see Fig. 3) and would explain the complicated OH velocity pattern seen at MERLIN resolution.

5. Conclusions

The flux density of the central line emission features of the single-dish emission of Mrk 273 has been mostly recovered in a region of around 108 pc at the eastern of the northern radio components. The distinct velocity pattern and spectral shape of the maser spectrum indicates that the emission originates in an almost edge-on disk or torus covering the radio source.

Observational data from various wavelength regimes do not yet provide a completely consistent picture of the nature of the nuclear power plant in the northern nucleus.

In the infrared, the total extent of the northern nucleus can be determined by either a single gray-body emission area of about 418 pc or a blackbody emission area of about 340 pc. These estimates are remarkably consistent with the maximum extent of 370 pc found for the radio continuum by the VLBA array and suggest that star-formation is taking place on these scale sizes (Carilli & Taylor 2000). In addition, EVN observation and other at higher resolution show a distinct region of enhanced continuum emission located in the central part in the northern nucleus of maximal 157 pc in extent. The combined presence of these two distinct morphologies indicates that both a starburst and an active galactic nucleus are present in the northern nucleus of Mrk 273, which is optically classified as a LINER 1. In addition, the northern nucleus shows exclusively hard X-ray emission indicating either a heavily obscured high-luminosity AGN or a low-luminosity AGN that mimics a LINER 1 spectrum with photo-ionization due to hard photons (Terashima et al. 2000). The HI column density that is required to block the entire soft X-ray emission towards the northern region is $4.1 \times 10^{23} \text{ cm}^{-2}$, which is quite similar to estimates in the mid-infrared bands of $\sim 5 \times 10^{23} \text{ cm}^{-2}$ (Xia et al. 2002). Nevertheless, the HI column density seen towards the individual continuum components in the northern region is significantly lower with a value of $T_s \times (1.8 \pm 0.3) 10^{20} \text{ cm}^{-2}$. These estimates could only be similar for an unlikely spin temperature of about 2300 K, which is an order of magnitude higher than the estimates of spin temperatures based on a galactic gas-to-dust ratio and an optical extinction similar to those detected in NGC 4945 or SgrA* (Xia et al. 2002; Carilli & Taylor 2000). On the other hand, the OH column density $N_{\text{OH}} = 4.58 \times 10^{14} T_{\text{ex}} \text{ cm}^{-2}$ observed towards the north-eastern source and the standard galactic HI to OH abundance ratio implies a low line-of-sight obscuration (Mann & Williams 1980). Therefore, the OH maser emission combined with the steep radio spectral index indicates the presence of a low luminosity AGN seen through a highly ionized screen at the northern nucleus. The binding mass of the central object in the north-eastern component is determined by Keplerian kinematics and is on the order of $(1.39 \pm 0.16) \times 10^9 M_{\odot}$. This is two orders of magnitudes larger than the binding mass traced by the H₂O Megamaser emission in the galaxy NGC 4258 (Greenhill et al. 1995).

The spatial structure, spectral signature, and velocity pattern of the OH emission in Mrk 273 at resolution of a few tens of parsec clearly reveal an edge-on disk with Keplerian kinematics in the northern nucleus. The distinct velocity pattern of the disk would represent a kinetically independent structure in this nucleus, which does not agree with the presence of an east-west elongated nuclear disk or torus as traced by HI in absorption in the northern region (Cole et al. 1999). However, the observed OH velocity gradient is comparable to the gradient of the HI absorption, which shows evidence for solid-body rotation and appears non-consistent with the other evidence. Alternatively, this component could also be explained by radial outflow.

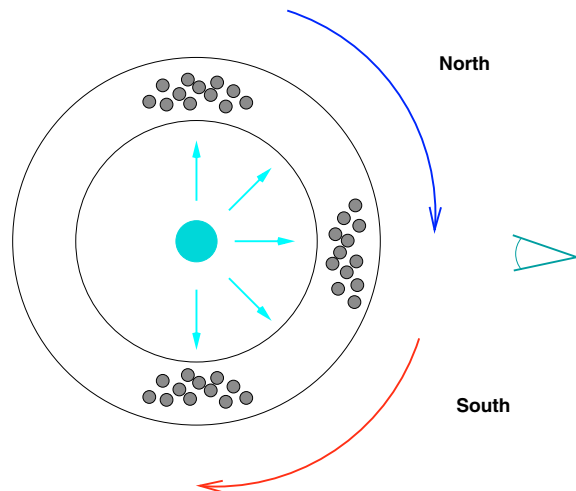


Fig. 8. Schematic view of the maser emission seen with the EVN observation. The relative amplification of the model maser emission depends on the ratio of the OH column densities to the OH velocity dispersion. At the top and bottom of the nuclear disk, the line-of-sight column densities are relatively high with respect to the centre, which is compensated by specific rotation velocities and different line-of-sight dispersions. This scenario accounts for the weaker and broader line features f_2 and f_4 and the central strong narrow line feature f_3 of the 1667 MHz emission in Fig. 4.

The missing maser emission between the WSRT and the EVN observations accounts for 80 percent of the total OH emission in Mrk 273. Corresponding line features in the MERLIN observations show that the OH emission traces a complex and disturbed velocity structure at larger scale sizes (Knapen et al. 1997). The question remains whether the velocity field of the large scale HI absorption signifies rotation or radial outflow. Alternatively the western component of the northern nucleus, with its marginal narrow OH emission component, its broad HI absorption feature, and its thermal spectral index, may be interpreted as a region with enhanced star formation rather than a second nucleus (Carilli & Taylor 2000).

The favored scenario for the northern nucleus is a combination of star-formation that produces starburst driven winds, resulting in high offset line features, and a low luminosity AGN obscured by a dusty disk of 108 pc in extent producing a highly disturbed gas region that mimics a LINER spectrum. It should be noted that the hydroxyl maser emission in Mrk 273 shows no saturation effects at kilo parsec and parsec scale sizes. This is in contrast with the compact maser components discovered in high-resolution observations of other bright OH Megamaser sources, such as Arp 220, IRAS 17208–0014, and III Zw 35 (Lonsdale et al. 1998; Diamond et al. 1999). In these sources saturation and non-saturation has been concluded on the basis of the compactness of the OH emission with respect to the continuum. The current EVN observations show for the first time that compact OH emission does remain unsaturated. It has also been shown that the total OH maser emission at galactic size scales results from an unsaturated maser process working with a pumping efficiency of only a few one-thousands. Such low conversion efficiencies have been found for most of the OH Megamaser galaxies, which indicates that saturation

effects may not play a significant role after all and support a Megamaser model based on amplification of background radio continuum by foreground molecular gas (Baan 1985, 1989; Klöckner 2004).

Acknowledgements. The European VLBI Network is a joint facility of European, Chinese, South African and other radio astronomy institutes funded by their national research councils. The Westerbork Synthesis Radio Telescope is operated by the ASTRON (Netherlands Foundation for Research in Astronomy) with support from the Netherlands Foundation for Scientific Research (NWO). The authors thank M. Elitzur for fruitful discussions on maser emission.

References

- Baan, W. A. 1985, *Nature*, 315, 26
 Baan, W. A. 1989, *ApJ*, 338, 804
 Baan, W. A., Haschick, A. D. 1984, *ApJ*, 279, 541
 Baan, W. A., Haschick, A. D., & Henkel, C. 1989, *ApJ*, 346, 680
 Baan, W. A., Rhoads, J., Fisher, K., Altschuler, D. R., & Haschick, A. 1992, *ApJ*, 396, L99
 Baan, W. A., Wood, P. A. D., & Haschick, A. D. 1982, *ApJ*, 260, L49
 Carilli, C. L., & Taylor, G. B. 2000, *ApJ*, 532, L95
 Charlot, P., Campbell, R. M., Alef, W., et al. 2002, in *Proc. of the 5th European VLBI Network Symposium, Gustav–Stresemann–Institut, Bonn, Germany*, ed. E. Ros, R. W. Porcas, A. P. Lobanov, & J. A. Zensus, 9
 Cole, G. H. J., Pedlar, A., Holloway, A. J., & Mundell, C. G. 1999, *MNRAS*, 310, 1033
 Colina, L., Arribas, S., & Borne, K. D. 1999, *ApJ*, 527, L13
 Condon, J. J. 1992, *ARA&A*, 30, 575
 Crawford, T., Marr, J., Partridge, B., & Strauss, M. A. 1996, *ApJ*, 460, 225
 Destombes, J. L., Marliere, C., Baudry, A., & Brillet, J. 1977, *A&A*, 60, 55
 Diamond, P. J., Lonsdale, C. J., Lonsdale, C. J., & Smith, H. E. 1999, *ApJ*, 511, 178
 Downes, D., & Solomon, P. M. 1998, *ApJ*, 507, 615
 Elitzur, M. 1992, *Astronomical masers. Astronomical masers Kluwer Academic Publishers (Astrophysics and Space Science Library)*, 170, 365
 Güsten, R. 1989, in *The Center of the Galaxy, IAU Symp.*, 136, 89
 Goss, W. M. 1968, *ApJS*, 15, 131
 Greenhill, L. J., Jiang, D. R., Moran, J. M., et al. 1995, *ApJ*, 440, 619
 Henkel, C., & Wilson, T. L. 1990, *A&A*, 229, 431
 Klaas, U., Haas, M., Müller, S. A. H., et al. 2001, *A&A*, 379, 823
 Klöckner, H. R. 2004, Ph.D. Thesis, Rijksuniversiteit Groningen
 Klöckner, H. R., Baan, W. A., & Garrett, G. A. 2003, *Nature*, 421, 821
 Klöckner, H. R., & Baan, W. A. 2002, in *Proc. of the 5th European VLBI Network Symposium, Gustav–Stresemann–Institut, Bonn, Germany*, ed. E. Ros, R. W. Porcas, A. P. Lobanov, & J. A. Zensus, 175
 Klöckner, H. R., & Baan, W. A. 2003, in *JENAM 2002 - The unsolved universe: Challenges for the future, Porto, Portugal*, ed. M. J. P. F. G. Monteiro
 Knapen, J. H., Laine, S., Yates, J. A., et al. 1997, *ApJ*, 490, L29
 Lonsdale, C. J., Lonsdale, C. J., Diamond, P. J., & Smith, H. E. 1998, *ApJ*, 493, L13
 Mann, A. P. C., & Williams, D. A. 1980, *Nature*, 283, 721
 Pihlström, Y. M., Conway, J. E., Booth, R. S., Diamond, P. J., & Polatidis, A. G. 2001, *A&A*, 377, 413
 Rogers, A. E. E., & Barrett, A. H. 1968, *ApJ*, 151, 163
 Sanders, D. B., & Mirabel, I. F. 1996, *ARA&A*, 34, 749
 Schmelz, J. T., Baan, W. A., & Haschick, A. D. 1987, *ApJ*, 321, 225
 Schmelz, J. T., Baan, W. A., & Haschick, A. D. 1988, *ApJ*, 329, 142
 Skinner, C. J., Smith, H. A., Sturm, E., et al. 1997, *Nature*, 386, 472
 Staveley-Smith, L., Norris, R. P., Chapman, J. M., et al. 1992, *MNRAS*, 258, 725
 Terashima, Y., Ho, L. C., & Ptak, A. F. 2000, *ApJ*, 539, 161
 Xia, X. Y., Xue, S. J., Mao, S., et al. 2002, *ApJ*, 564, 196
 Yates, J. A., Richards, A. M. S., Wright, M. M., et al. 2000, *MNRAS*, 317, 28
 Yun, M. S., Reddy, N. A., & Condon, J. J. 2001, *ApJ*, 554, 803